

This is an Open Access document downloaded from ORCA, Cardiff University's institutional repository: <https://orca.cardiff.ac.uk/id/eprint/100519/>

This is the author's version of a work that was submitted to / accepted for publication.

Citation for final published version:

Dosso, Jacopo , Tasseroul, Jonathan, Fasano, Francesco, Marinelli, Davide, Biot, Nicolas, Fermi, Andrea and Bonifazi, Davide 2017. Synthesis and optoelectronic properties of hexa-peri -hexabenzoborazinocoronene. *Angewandte Chemie International Edition* 56 (16) , pp. 4483-4487. 10.1002/anie.201700907

Publishers page: <http://dx.doi.org/10.1002/anie.201700907>

Please note:

Changes made as a result of publishing processes such as copy-editing, formatting and page numbers may not be reflected in this version. For the definitive version of this publication, please refer to the published source. You are advised to consult the publisher's version if you wish to cite this paper.

This version is being made available in accordance with publisher policies. See <http://orca.cf.ac.uk/policies.html> for usage policies. Copyright and moral rights for publications made available in ORCA are retained by the copyright holders.



# Synthesis and Optoelectronic Properties of Hexa-*peri*-hexabenzoborazinocoronene

Jacopo Dosso, Jonathan Tasseroul, Francesco Fasano, Davide Marinelli, Nicolas Biot, Andrea Fermi, and Davide Bonifazi\*

**Abstract:** The first rational synthesis of a BN-doped coronene derivative in which the central benzene ring has been replaced by a borazine core is described. This includes six C–C ring-closure steps that, through intramolecular Friedel–Crafts-type reactions, allow the stepwise planarization of the hexaarylborazine precursor. UV/Vis absorption, emission, and electrochemical investigations show that the introduction of the central BN core induces a dramatic widening of the HOMO–LUMO gap and an enhancement of the blue-shifted emissive properties with respect to its all-carbon congener.

Graphene is one of the leading materials in today's science,<sup>[1]</sup> but the lack of a band gap limits its application to replace semiconductors in optoelectronic devices.<sup>[2]</sup> To overcome this limitation, the replacement of C=C bonds by isostructural and isoelectronic bonds such as polar B=N<sup>[3]</sup> is emerging as an effective strategy to open a band gap in monoatomic graphene layers.<sup>[4]</sup> To the best of our knowledge, only one example of a BN-doped covalent network featuring a regular doping pattern has been described so far through surface-assisted reaction.<sup>[5]</sup> Otherwise, only sheets containing B, N and C (h-BNC) over wide compositional ranges randomly distributed in domains of h-BN and graphitic phases have been prepared so far.<sup>[6]</sup> At the molecular level, notable examples include BN-doped polycyclic aromatic hydrocarbons.<sup>[7]</sup> Among those, the isolation of the first hexa-*peri*-hexabenzoborazinocoronene (HBBNC)<sup>[8]</sup> from pyrolysis of a borazine precursor by Bettinger and co-workers is an important example in view of the creation of hybrid graphenes featuring controlled BN-doping patterns (Figure 1). However, the stunted solubility of this molecule limited in-depth structural and physical studies.

Herein we describe the first rational synthesis of B<sub>3</sub>N<sub>3</sub>-doped benzocoronene 1 that, being soluble in common organic solvents, allowed a direct comparison of optoelectronic properties with those of its full-carbon congener. Generally, controlled BN-doping patterns in PAHs are

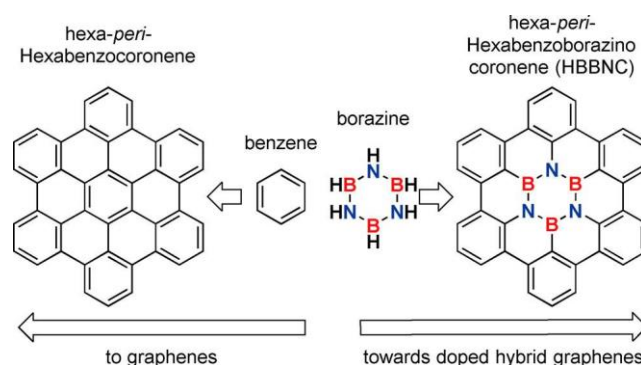
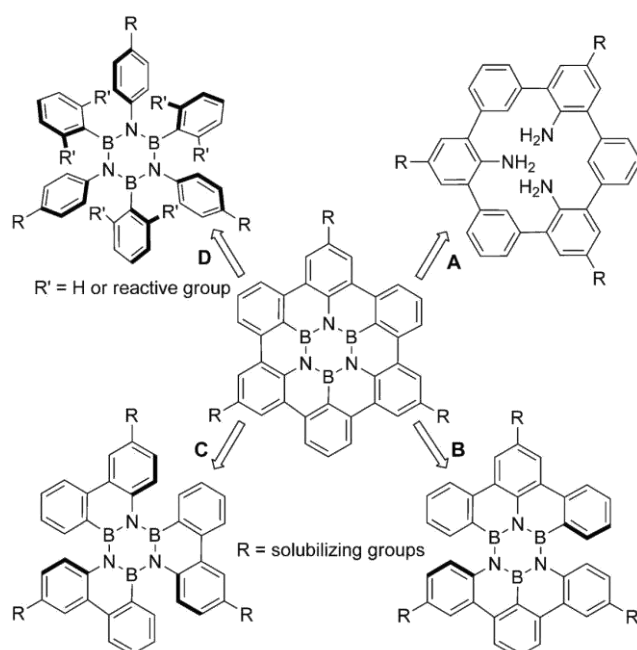


Figure 1. HBC and its borazino-doped analogue HBBNC.

obtained through bottom-up synthesis involving aniline-type precursors<sup>[3]</sup> that undergo planarization through intramolecular electrophilic aromatic substitution reactions, simultaneously forming C–B and B–N bonds in the presence of BCl<sub>3</sub> and a Lewis acid. At the synthetic planning level, this consideration guided us to contemplate at first a convergent path relegating the formation of the HBBNC core to the last step (Scheme 1, path A). However, the scarce yield for preparing the triamino-spherand precursor forced us to defer this synthetic path and to anticipate the B<sub>3</sub>N<sub>3</sub> formation in an earlier step.



[\*] J. Dosso, F. Fasano, D. Marinelli, N. Biot, Dr. A. Fermi, Prof. Dr. D. Bonifazi

School of Chemistry, Cardiff University, Main Building Park Place, Cardiff CF10 3AT (UK)

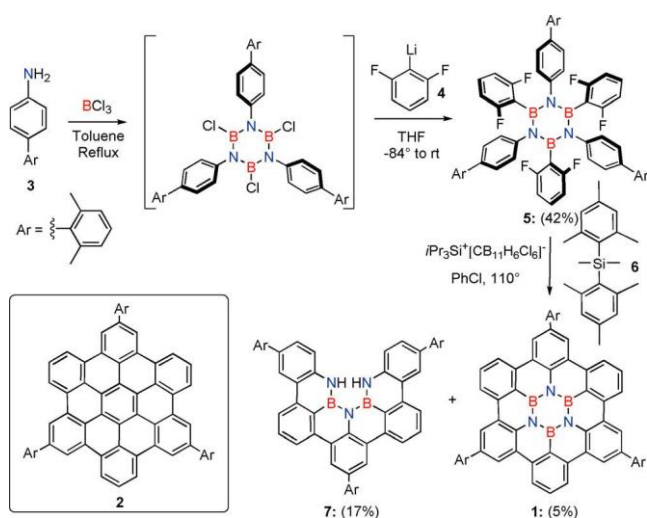
E-mail: bonifazi@cardiff.ac.uk

Dr. J. Tasseroul, Prof. Dr. D. Bonifazi

Department of Chemistry, University of Namur (UNamur)  
Rue de Bruxelles 61, Namur 5000 (Belgium)

This would lead to the HBBNC core through two, three or six ring-closure reactions involving the aryl substituents (Scheme 1, paths B, C, and D). As we have predicted a potential instability of the strained borazine precursors<sup>[9]</sup> of paths B and C, a decision was made to undertake plan D. Commonly, the planarization of covalently preorganized aryl moieties into PAHs is obtained through Scholl-type oxidative ring-closure reactions.<sup>[2b, 10]</sup> However, the vulnerability of the borazine ring under oxidative conditions<sup>[11, 3d]</sup> directed us to consider a Friedel–Crafts-type substitution as the planarization reaction. This line of thought led us back to hypothetical borazine precursors bearing appropriate leaving groups (LG) at the *ortho* positions of the B-aryl substituents (path D) that, triggered under given conditions, can yield reactive arylum species. It is hard to not notice that the presence of *ortho* LG additionally exerts protection to the B-atom centers, making the borazine precursor enough stable to be handled. Embracing this synthetic strategy, we prepared a borazine precursor bearing F and peripheral xyllyl moieties as LGs and solubilizing groups, respectively.

Following previous procedures,<sup>[12]</sup> hexafluoro borazine 5 was thus obtained after reaction of 4-xyllyl aniline 3 with BCl<sub>3</sub> upon subsequent addition of difluoro-ArLi 4 (Scheme 2). A crystal of borazine 5, suitable for X-ray diffraction, was



Scheme 2. Synthetic path for preparing xyllyl-substituted HBBNC 1; full-carbon congener 2.<sup>[13]</sup>

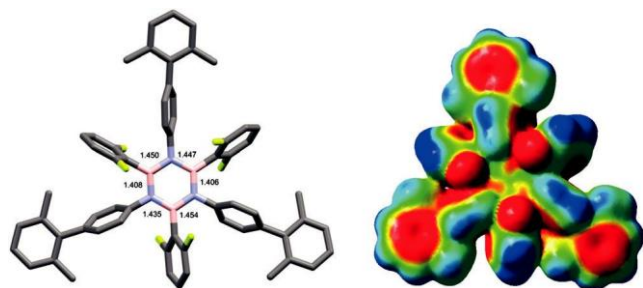


Figure 2. X-ray structure and ESP mapped on the vdW surface up to an electron density of 0.001 electron bohr<sup>3</sup> for 5. B pink, N blue, F green, C gray; space group: P2<sub>1</sub>/c. B N distances in Å are shown.<sup>[19]</sup>

obtained by vapor diffusion of MeOH to a CH<sub>2</sub>Cl<sub>2</sub> solution of 5 (Figure 2). The quasi-orthogonal arrangement of the aryl moieties forces the F substituents to nest atop the B atoms (B...F = 2.922 Å), negatively shielding the electrophilic center. Capitalizing on the Friedel–Crafts ring-closure reaction of fluoroarenes developed by Siegel and co-workers,<sup>[14]</sup> borazine 5 could be planarized into HBBNC 1 (5 % yield, 61 % per C C bond formation) in the presence of [iPr<sub>3</sub>Si...CB<sub>11</sub>H<sub>6</sub>Cl<sub>6</sub>] and Me<sub>2</sub>SiMes<sub>2</sub> at 110 °C in PhCl operating in a Schlenk line. Together with HBBNC 1, partially fused BN-derivative 7 was obtained as major product (17 % yield), suggesting that the ring closure proceeds stepwise with the last aryl fusion likely being the rate-determining step. All-carbon congener HBC 2 (Scheme 2) was also prepared for comparison purposes (Supporting Information, Scheme S1).<sup>[13]</sup>

Molecule 1 was characterized using NMR, UV/Vis, and IR spectroscopy and HR-MALDI spectrometry. At first, HBBNC 1 was unambiguously identified by HR-MALDI through the detection of the peak corresponding to the molecular ion at m/z 837.3652 (C<sub>60</sub>H<sub>42</sub>B<sub>3</sub>N<sub>3</sub><sup>+</sup>, calc.: 837.3658). Solution <sup>1</sup>H-NMR spectra further confirmed the structure of HBBNC 1 (Figure 3 B). Specifically, coupled H<sub>a</sub> and H<sub>b</sub>

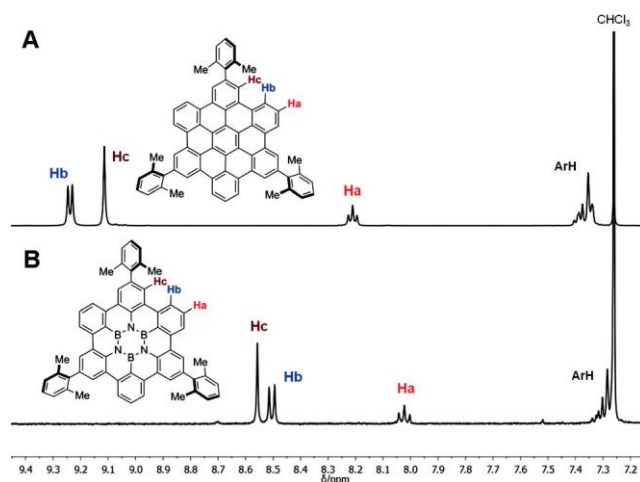


Figure 3. Exerts of the <sup>1</sup>H-NMR spectra (400 MHz, CDCl<sub>3</sub>) in the aromatic region for HBBNC 1 (bottom) and HBC 2 (above).

protons appear as triplet (8.05 ppm) and doublet (8.55 ppm), respectively, whereas one singlet (8.58 ppm) is observed for H<sub>c</sub> proton. An analogous resonance pattern (Figure 3 A) is also observed for reference 2. Notably, the presence of the inner B<sub>3</sub>N<sub>3</sub> cycle in 1 induces a high-field shift of the proton resonances with respect to those of 2, suggesting a significant decrease of the magnetic anisotropic properties of the B<sub>3</sub>N<sub>3</sub>-doped derivative. Analogously, a remarkable high-field shift was also observed for the boron resonance (at 30.59 ppm) in the <sup>11</sup>B-NMR spectrum (Supporting Information, Figure S24) of 1 when compared to that of precursor 5 (at 34.9 ppm).

To further corroborate the chemical structure of 1, crystals suitable for X-ray diffraction analysis were obtained by vapour diffusion of iPrOH to a C<sub>6</sub>H<sub>6</sub> solution of 1 (Figure 4 A).

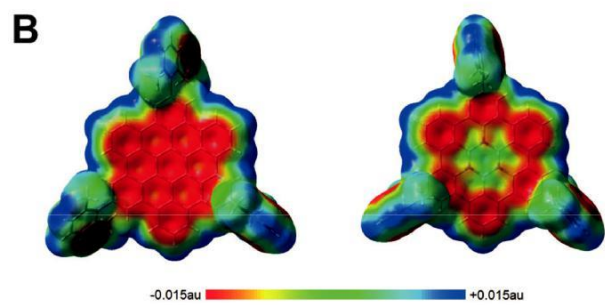
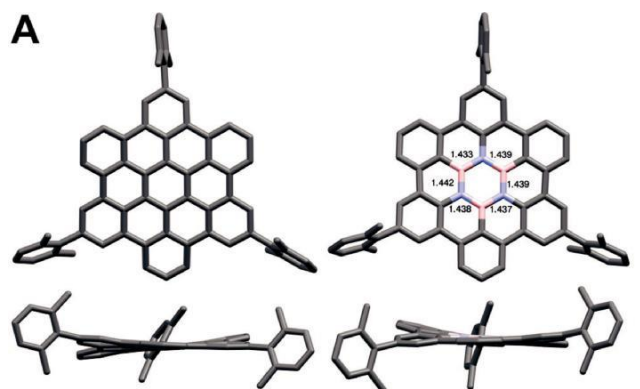


Figure 4. A) Horizontal (top) and side (bottom) view of the X-ray crystal structures of HBBNC (with the B N distances in Å) 1 (right) and HBC 2 (left). B pink, N blue, C gray; space groups:  $I2/a$  and  $P1$ , respectively. B) ESP mapped on the vdW surface up to an electron density of 0.001 electron bohr<sup>3</sup>.<sup>[19]</sup>

The X-ray analysis confirms the nearly flat shape of the BNC framework, displaying a similar structure to that of all-carbon congener 2, with shorter B N lengths (1.433–1.442 Å, Figure 4 A) than those measured in hexagonal boron nitride (h-BN, 1.446 Å). To appraise the effect of the BN doping on the aromatic p-surface, we further determined the charge distribution of the crystal structure of 1 in the form of ESP (Figure 4 B) calculated with Gaussian 09 at B3LYP/6-31G-(d,p) level of theory (Supporting Information).

As expected, the p-surface of 2 is negatively charged showing the presence of a homogenous p-cloud above and below the HBC skeleton. On the

other hand, 1 displays a great charge polarization of the p-surface, with the N and B atoms negatively and positively charged, respectively, and the outer hexaphenylene rim negatively charged. These results are consistent with the expected ambipolar character of the molecule.<sup>[15]</sup> UV/Vis absorption and emission properties in  $\text{CH}_2\text{Cl}_2$  of molecules 1 and 2 are displayed in Figure 5 and Table 1. The lowest-energy electronic transition of 1 appears in the near-UV (375 nm) at significantly higher energy with respect to that of 2 (446 nm). In line with theoretical predictions,<sup>[4a,b, 11]</sup>

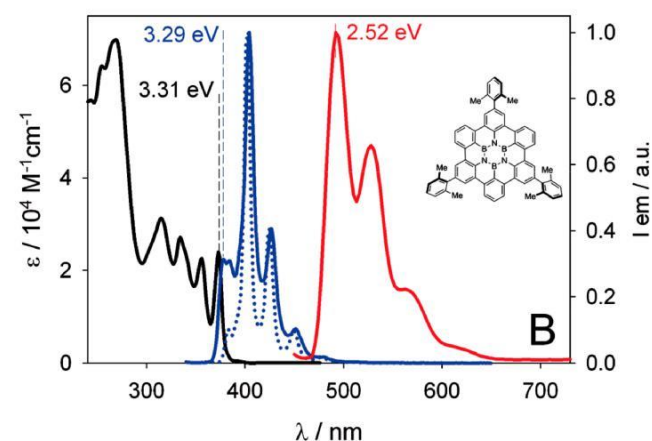
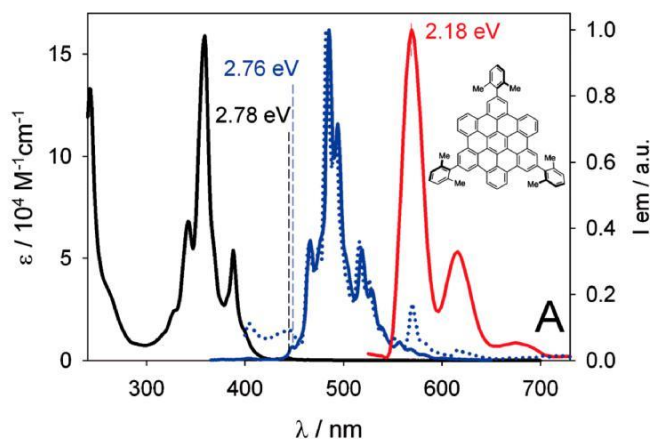


Figure 5. Absorption (black) and normalized fluorescence (blue) spectra of 1 (B,  $\lambda_{\text{exc}}=315$  nm) and 2 (A,  $\lambda_{\text{exc}}=355$  nm) in air equilibrated  $\text{CH}_2\text{Cl}_2$  at RT; fluorescence (blue dotted) and phosphorescence (red) spectra at 77 K in a  $\text{CH}_2\text{Cl}_2$  :  $\text{CH}_3\text{OH}$  (1:1, v/v) rigid matrix.

this finding suggests that the  $\text{B}_3\text{N}_3$ -doping widens the molecular optical band gap ( $\text{DE}_{\text{opt}} = 0.53$  eV). Furthermore, the absorption bands of 1 show noticeable vibrational substructures evidencing a high degree of rigidity of the molecular skeleton.<sup>[16]</sup>

Table 1: Photophysical data for 1 and 2 in solution and at the solid state.

Molecule	Absorption				Emission		
	$\lambda$ [nm] ( $\epsilon$ , L mol <sup>-1</sup> cm <sup>-1</sup> ) <sup>[a]</sup>	$\lambda_{\text{max,fl}}$ [nm]	$E_{\text{opt,fl}}$ [eV] <sup>[b]</sup>	$t_{\text{fl}}$ [ns]	$F_{\text{fl}}$ <sup>[c]</sup>	$\lambda_{\text{max,PH}}$ [nm] <sup>[d]</sup>	$t_{\text{ph}}$ [s] <sup>[d]</sup>
2 ( $\text{CH}_2\text{Cl}_2$ )	446 (1000)	485 <sup>[a]</sup>	2.76	16.4 <sup>[a]</sup>	0.03 <sup>[a]</sup>	570	0.8
	388 (53 800)			27.9 <sup>[f]</sup>			
	358 (159 100)						
2 (solid)	–	487	–	3.7 (64 %)	–	–	–
				12.1 (36 %) <sup>[e]</sup>			
1 ( $\text{CH}_2\text{Cl}_2$ )	375 (24 000)	404 <sup>[a]</sup>	3.29	8.2 <sup>[a]</sup>	0.43 <sup>[a]</sup>	492	4.0
	314 (31 200)			10.9 <sup>[f]</sup>			
1 (solid)	–	426	–	1.5 (43 %)	–	–	–
				8.0 (57 %) <sup>[e]</sup>			

[a] Recorded in air-equilibrated  $\text{CH}_2\text{Cl}_2$  at RT. [b] Calculated from the higher-energy maxima of the emission spectra in air-equilibrated  $\text{CH}_2\text{Cl}_2$  at RT ( $E_{\text{opt}}=1240/\lambda_{\text{fl}}$ ). [c] Quinine sulfate in 0.5 m  $\text{H}_2\text{SO}_4$  was used as the standard ( $F_{\text{QS}}=0.546$ ). [d] Recorded in a 1:1  $\text{CH}_2\text{Cl}_2$  :  $\text{CH}_3\text{OH}$  v/v rigid matrixes at 77 K (Supporting Information, Figure S31). [e] Fitting of the emission decays. Values in [%] indicate the weight of each exponential component in the biexponential fitting. [f] Calculated for  $\text{O}_2$ -free solutions.

Consistently, the emission spectra (Figure 5) in solution at room temperature reflect the same trend, with the intense emission peak of 1 ( $I_{\max} = 404$  nm,  $F_{\text{fl}} = 0.43$ ) significantly blue-shifted with respect to that of 2 ( $I_{\max} = 485$  nm). Notably, the  $F_{\text{fl}}$  value significantly increases to 0.77 in  $O_2$ -free solutions. Phosphorescence spectra at low temperature (Figure 5) showed long-lasting emission profiles ( $t_{\text{Phos}} = 4$  s) with 1 providing the highest-energy triplet emission ( $I_{\max, \text{Phos}} = 492$  and 570 nm for 1 and 2, respectively).<sup>[17]</sup> Furthermore, 1 displays appreciable solid-state fluorescence

emission in the violet–blue region ( $I_{\max} = 426$  nm vs.  $I_{\max} = 487$  nm for 2) at room temperature (Supporting Information, Figure S32).

Cyclic voltammetry (CV) measurements showed a quasi-reversible first oxidation wave at approximately 1.46 V vs. SCE in  $CH_2Cl_2$  for HBBNC 1 (Figure 6; Supporting Infor-

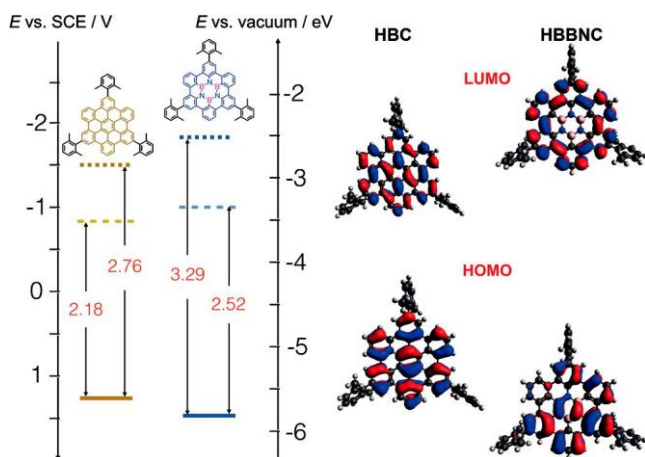


Figure 6. Left: Frontier orbital energies estimated from the CV and photophysical data for 1 and 2. Reduction potentials of the triplet excited states are evidenced by the narrower optical energy gaps ( $E^{T^*} = E^{1/2_{\text{ox}}} - E_{\text{opt}}^T$ ).  $F_c^+/F_c = 0.46$  V vs. SCE; 4.8 eV vs. vacuum. Right: HOMO and LUMO profiles for 1 and 2 at B3LYP/6-31G(d,p) level of theory (GAUSSIAN09).

mation, Figure S34), which is considerably higher in energy with respect to that of its carbon congener ( $E_{1/2_{\text{ox}}} = 1.27$  V vs. SCE).<sup>[18]</sup> On the other hand, no relevant reduction waves were detected at any scan rates under the same experimental conditions for both molecules. Taken together, these data allowed us to estimate the energies of the HOMO and LUMO orbitals, resulting to be 5.80 (HOMO) and 2.51 eV (LUMO) for 1 and 5.61 (HOMO) and 2.85 eV (LUMO) for 2 (Figure 6; Supporting Information, Table S4). To shed further light on the structure-property relation, we calculated the HOMO and LUMO orbitals for 1 and 2 (Figure 6; Supporting Information, Figure S35). As observed by others,<sup>[4a,b, 11]</sup> it transpires that both orbitals are homogeneously distributed on the p-surface of 2, whereas the LUMO for 1 is only located on the hexaphenylene rim. This suggests that the one-electron reduction of 1 is likely to be confined on the hexaphenylene periphery excluding the  $B_3N_3$  ring, whereas that of 2 is localized on the entire carbon p-surface.

In conclusion, we have described the first synthetic methodology to prepare a soluble HBBNC molecule following a planarization strategy based on a Friedel–Crafts reaction. This involves the simultaneous formation of six C–C bonds starting from a hexafluoroborazine precursor. First, X-ray diffraction confirmed the presence of the inner  $B_3N_3$  cycle, with short B–N bond lengths. The remarkable UV absorption, strong blue–violet singlet emission, and green phosphorescence of this class of hybrid  $B_3N_3$ -doped molecules are in line with the theoretical predictions. Given the importance and ubiquity of graphene in scientific research, the development of novel synthetic strategies leading to hybrid graphene derivatives featuring precise doping patterns will undoubtedly lead to new discoveries and applications in materials science. In this respect, the synthesis and photo-physical study of this long-awaited compound marks an important milestone toward the understanding of the optoelectronic properties of doped molecular graphenes.

## Acknowledgements

D.B. gratefully acknowledges the EU through the ERC Starting Grant “COLORLANDS” project. J.T. thanks the FRS-FNRS for his FRIA doctoral fellowship. The authors also acknowledge the use of the Advanced Computing @Cardiff (ARCCA) at Cardiff University, and associated support services.

## Conflict of interest

The authors declare no conflict of interest.

Keywords: borazine · boron nitrides · heteroatom doping · hexabenzocoronenes · polycyclic aromatic hydrocarbons

- [1] a) S. Park, R. S. Ruoff, *Nat. Nanotechnol.* 2009, 4, 217 – 224; b) F. Schwierz, *Nat. Nanotechnol.* 2010, 5, 487 – 496.
- [2] a) J. Wu, W. Pisula, K. Müllen, *Chem. Rev.* 2007, 107, 718 – 747; b) A. Narita, X. Wang, X. Feng, K. Müllen, *Chem. Soc. Rev.* 2015, 44, 6616 – 6643.
- [3] a) Z. Liu, T. B. Marder, *Angew. Chem. Int. Ed.* 2008, 47, 242 – 244; *Angew. Chem.* 2008, 120, 248 – 250; b) P. G. Campbell, A. J. V. Marwitz, S.-Y. Lui, *Angew. Chem. Int. Ed.* 2012, 51, 6074 – 6092; *Angew. Chem.* 2012, 124, 6178 – 6197; c) X. Wang, J. Wang, J. Pei, *Chem. Eur. J.* 2015, 21, 3528 – 3539; d) D. Bonifazi, F. Fasano, M. M. Lorenzo-Garcia, D. Marinelli, H. Oubaha, J. Tasseroul, *Chem. Commun.* 2015, 51, 15222 – 15236; e) H. Helten, *Chem. Eur. J.* 2016, 22, 12972 – 12982.
- [4] a) W. Xie, T. Yanase, T. Nagahama, T. Shimada, *C* 2016, 2, 2; b) N. Otero, K. E. El-kelany, C. Pouchan, M. R rat, P. Karama-nis, *Phys. Chem. Chem. Phys.* 2016, 18, 25315 – 25328; c) N. Otero, P. Karamanis, K. E. El-Kelany, M. R rat, L. Maschio, B. Civalieri, B. Kirtman, *J. Phys. Chem. C* 2017, 121, 709 – 722.
- [5] C. SQuchez-SQuchez, S. Br4ller, H. Sachdev, K. Müllen, M. Krieg, H. F. Bettinger, A. Nicola', V. Meunier, L. Talirz, R. Fasel, P. Ruffieux, *ACS Nano* 2015, 9, 9228 – 9235.

- [6] a) L. Ci, L. Song, C. Jin, D. Jariwala, D. Wu, Y. Li, A. Srivastava, *Nat. Mater.* 2010, 9, 430 – 435; b) C. Huang, C. Chen, M. Zhang, L. Lin, X. Ye, S. Lin, M. Antonietti, X. Wang, *Nat. Commun.* 2015, 6, 7698 – 7704.
- [7] Selected examples: a) G. C. Culling, M. J. S. Dewar, P. A. Marr, *J. Am. Chem. Soc.* 1964, 86, 1125 – 1127; b) D. J. H. Emslie, W. E. Piers, M. Parvez, *Angew. Chem. Int. Ed.* 2003, 42, 1096 – 1109; *Angew. Chem.* 2003, 115, 1290 – 1293; c) C. A. Jaska, D. J. Emslie, M. J. Bosdet, W. E. Piers, *J. Am. Chem. Soc.* 2006, 128, 10885 – 10896; d) M. J. D. Bosdet, C. A. Jaska, W. E. Piers, T. S. Sorensen, *Org. Lett.* 2007, 9, 1395 – 1398; e) M. J. D. Bosdet, W. E. Piers, T. S. Sorensen, M. Parvez, *Angew. Chem. Int. Ed.* 2007, 46, 4940 – 4943; *Angew. Chem.* 2007, 119, 5028 – 5031; f) A. J. V. Marwitz, M. H. Matus, L. N. Zakharov, D. A. Dixon, S.-Y. Liu, *Angew. Chem. Int. Ed.* 2009, 48, 973 – 977; *Angew. Chem.* 2009, 121, 991 – 995; g) T. Hakeyama, S. Hashimoto, S. Seki, M. Nakamura, *J. Am. Chem. Soc.* 2011, 133, 18614 – 18617; h) J. S. A. Ishibashi, J. L. Marshall, A. Mazie, G. J. Lovinger, B. Li, L. N. Zakharov, A. Dargelos, A. Gracia, A. Chrostowska, S. Liu, *J. Am. Chem. Soc.* 2014, 136, 15414 – 15421; i) G. A. Molander, S. R. Wisniewski, *J. Org. Chem.* 2014, 79, 6663 – 6678; j) H. Braunschweig, M. A. Celik, F. Hupp, I. Krumme-nacher, L. Mail nder, *Angew. Chem. Int. Ed.* 2015, 54, 6347 – 6351; *Angew. Chem.* 2015, 127, 6445 – 6449; k) X. Wang, F. Zhang, K. S. Schellhammer, P. Machata, F. Ortman, G. Cuniberti, Y. Fu, J. Hunger, R. Tang, A. A. Popov, R. Berger, K. M4llen, X. Feng, *J. Am. Chem. Soc.* 2016, 138, 11606 – 11615; l) M. Numano, N. Nagami, S. Nakatsuka, T. Katayama, K. Nakajima, S. Tatsumi, N. Yasuda, T. Hatakeyama, *Chem. Eur. J.* 2016, 22, 11574 – 11577.
- [8] a) M. Krieg, F. Reicherter, P. Haiss, M. Stṙbele, K. Eichele, J. Treanor, R. Schaub, H. F. Bettinger, *Angew. Chem. Int. Ed.* 2015, 54, 8284 – 8286; *Angew. Chem.* 2015, 127, 8402 – 8404; b) F. Ciccullo, A. Calzolari, I. P%<sup>s</sup>, S. A. Savu, M. Krieg, H. F. Bettinger, E. Magnano, T. Chass , M. B. Casu, *J. Phys. Chem. C* 2016, 120, 17645 – 17651.
- [9] S. Biswas, M. M4ller, C. Ṫnshoff, K. Eichele, C. Maichle-Ṁssmer, A. Ruff, B. Speiser, H. F. Bettinger, *Eur. J. Org. Chem.* 2012, 4634 – 4639.
- [10] M. D. Watson, A. Fechtenk̇tter, K. M4llen, *Chem. Rev.* 2001, 101, 1267 – 1300.
- [11] C. Ṫnshoff, M. M4ller, T. Kar, F. Latteyer, T. Chass , K. Eichele, H. F. Bettinger, *ChemPhysChem* 2012, 13, 1173 – 1181.
- [12] a) S. J. Groszos, S. F. Stafiej, *J. Am. Chem. Soc.* 1958, 80, 1357 – 1360; b) A. Wakamiya, T. Ide, S. Yamaguchi, *J. Am. Chem. Soc.* 2005, 127, 14859 – 14866; c) S. Kervyn, O. Fenwick, F. Di Stasio, Y. Sig Shin, J. Wouters, G. Accorsi, S. Osella, D. Beljonne, D. Bonifazi, *Chem. Eur. J.* 2013, 19, 7771 – 7779; d) S. Kervyn, N. Kalashnyk, M. Riello, B. Moreton, J. Tasseroul, J. Wouters, T. S. Jones, A. De Vita, G. Costantini, D. Bonifazi, *Angew. Chem. Int. Ed.* 2013, 52, 7410 – 7414; *Angew. Chem.* 2013, 125, 7558 – 7562.
- [13] R. Yamaguchi, S. Hiroto, H. Shinokubo, *Org. Lett.* 2012, 14, 2472 – 2475.
- [14] O. Allemann, S. Duttwyler, P. Romanato, K. K. Baldrige, J. S. Siegel, *Science* 2011, 332, 574 – 577.
- [15] E. Vessally, S. Soleimani-Amiri, A. Hosseinian, L. Edjlali, A. Bekhradnia, *Appl. Surf. Sci.* 2017, 396, 740 – 745.
- [16] X. Wang, F. Zhuang, R. Wang, X. Wang, X. Cao, J. Wang, J. Pei, *J. Am. Chem. Soc.* 2014, 136, 3764 – 3767.
- [17] S. Hashimoto, T. Ikuta, K. Shiren, S. Nakatsuka, J. Ni, M. Nakamura, T. Hatakeyama, *Chem. Mater.* 2014, 26, 6265 – 6271.
- [18] a) A. Stabel, P. Herwig, K. M4llen, J. P. Rabe, *Angew. Chem. Int. Ed. Engl.* 1995, 34, 1609 – 1611; *Angew. Chem.* 1995, 107, 1768 – 1770; b) R. Rathore, C. L. Burns, *J. Org. Chem.* 2003, 68, 4071 – 4074.
- [19] CCDC 1523993 (1), 1523994 (2), and 1523995 (5) contain the supplementary crystallographic data for this paper. These data are provided free of charge by The Cambridge Crystallographic Data Centre.

